Journal of Chromatography A, 1218 (2011) 427–440

Contents lists available at ScienceDirect

Journal of Chromatography A

journal homepage: www.elsevier.com/locate/chroma

Hydrophobic interaction chromatography of proteins. IV. Protein adsorption capacity and transport in preparative mode

Brian C.S. To[a,b,1], Abraham M. Lenhoff[b,*]

[a] Merck Research Laboratories, Sumneytown Pike, West Point, PA 19486, USA
[b] Department of Chemical Engineering, University of Delaware, Newark, DE 19716, USA

ARTICLE INFO

Article history:
Received 23 August 2010
Received in revised form
17 November 2010
Accepted 23 November 2010
Available online 27 November 2010

Keywords:
Phenyl adsorbents
Batch uptake
Column breakthrough
Diffusivities
Adsorption isotherms
Adsorption capacity

ABSTRACT

The adsorption isotherms of four model proteins (lysozyme, α-lactalbumin, ovalbumin, and BSA) on eight commercial phenyl hydrophobic interaction chromatography media were measured. The isotherms were softer than those usually seen in ion-exchange chromatography of proteins, and the static capacities of the media were lower, ranging from 30 to 110 mg/mL, depending on the ammonium sulfate concentration and the protein and adsorbent types. The protein-accessible surface area appears to be the main factor determining the binding capacity, and little correlation was seen with the protein affinities of the adsorbents. Breakthrough experiments showed that the dynamic capacities of the adsorbents at 10% breakthrough were 20–80% of the static capacities, depending on adsorbent type. Protein diffusivities in the adsorbents were estimated from batch uptake experiments using the pore diffusion and homogeneous diffusion models. Protein transport was affected by the adsorbent pore structures. Apparent diffusivities were higher at lower salt concentrations and column loadings, suggesting that adsorbed proteins may retard intraparticle protein transport. The diffusivities estimated from the batch uptake experiments were used to predict column breakthrough behavior. Analytical solutions developed for ion-exchange systems were able to provide accurate predictions for lysozyme breakthrough but not for ovalbumin. Impurities in the ovalbumin solutions used for the breakthrough experiments may have affected the ovalbumin uptake and led to the discrepancies between the predictions and the experimental results.

1. Introduction

Hydrophobic interaction chromatography (HIC) is attractive to the biotechnology and pharmaceutical industries because it is controlled by adsorption mechanisms that are different from those in ion-exchange chromatography and reverse-phase chromatography. Previous research in HIC has focused on understanding how different factors affect protein adsorption, while much less attention has been paid to protein transport in HIC media, which has an impact on design and scale-up in preparative chromatography. Protein diffusion in porous media is generally slower than in free solution due to hydrodynamic interactions between the protein and the pore walls [1], the tortuosity of the pore structure of the media [2] and steric exclusion of the protein molecules from the vicinity of the pore walls [3]. Only limited information on protein transport in HIC adsorbents is available in the literature. The pore diffusivities of α-chymotrypsinogen A in SnyChroprep propyl media [4], BSA in propyl-silica gel [5], and α-amylase in Duolite XAD-761 [6] have been measured via batch uptake or column breakthrough. Recently, the pore diffusivities of several model proteins in a set of HIC media were also estimated from pulse response experiments [7,8].

Although pulse response experiments provide a simple method to measure protein diffusivities in chromatographic media, they are usually performed in the linear region of the adsorption isotherm and include both adsorption and desorption steps. The coupling of protein transport and adsorption in preparative chromatography occurs under somewhat different conditions, since the protein is usually loaded into the adsorbent to levels approaching the full capacity. Therefore, protein surface coverage is high in preparative mode, which can result in pore constriction [9] and increased interactions between bound and free protein. As a result, intraparticle protein transport behavior could be different from that found in pulse response experiments. Batch uptake is a useful technique to estimate protein diffusivities in chromatographic media under such conditions, which are similar to those in frontal loading. In addition, the effects of the initial bulk concentration, hence the amount of protein bound, can be determined.

In this study, the adsorption isotherms and breakthough profiles of lysozyme (LYS), α-lactalbumin (ALC), ovalbumin (OVA) and

* Corresponding author. Fax: +1 302 831 1048.
E-mail address: lenhoff@udel.edu (A.M. Lenhoff).
[1] Current address: Bayer HealthCare Pharmaceuticals, 800 Dwight Way, Berkeley, CA 94710, USA.

0021-9673/$ – see front matter © 2010 Elsevier B.V. All rights reserved.
doi:10.1016/j.chroma.2010.11.051

Table 1
Base matrices, mean particle diameters, d_p, mean pore radii, R_p, protein-accessible surface areas, ϕ, and protein-accessible intraparticle porosities, ε_p, of phenyl media used.

Stationary phase	Base matrix	d_p (μm)	R_p (nm)	ϕ (m^2/mL media)			ε_p		
				LYS/ALA	OVA	BSA	LYS/ALA	OVA	BSA
Phenyl Sepharose FF HS	Agarose	34	27	58	52	44	0.84	0.78	0.69
Phenyl Sepharose FF LS	Agarose	90	27	55	49	42	0.81	0.74	0.66
Phenyl Sepharose HP	Agarose	90	39	49	44	37	0.81	0.76	0.68
Toyopearl phenyl 650S	Methacrylate	30	107	26	23	20	0.64	0.62	0.58
TSK-gel phenyl-5PW	Methacrylate	35	104	13	13	12	0.55	0.53	0.51
Fractogel EMD phenyl (S)	Methacrylate	30	45	27	22	18	0.31	0.29	0.27
Source 15PHE	PS-DVB	15	42	26	23	22	0.44	0.41	0.38
POROS 20 HP2	PS-DVB	20	301	8	8	8	0.60	0.59	0.58

bovine serum albumin (BSA) were measured in eight commercially available phenyl media. The pore and homogeneous diffusivities of the proteins were estimated from batch uptake experiments and used to calculate column breakthrough via three different breakthrough models. The calculated breakthrough curves were then compared with the experimental results to evaluate the validity of several analytical solutions for column breakthrough.

2. Theory

2.1. Adsorption isotherms

The estimation of effective protein diffusivities in chromatographic adsorbents from batch uptake experiments and the calculation of column breakthrough both involve coupled diffusion and adsorption and therefore require knowledge of the protein adsorption isotherms. In the context of coupled diffusion and adsorption, the isotherm equation is used only in a descriptive manner and its mechanistic basis is of minor importance. For example, although the Langmuir isotherm was developed for gas adsorption, it is commonly used for protein adsorption due to its simplicity and capability to fit some experimental results. Other isotherm models have also been developed to describe protein adsorption, with most emphasis on ion-exchange systems, including the steric mass action formalism [10] and the available area isotherm [11]. Some isotherms have been developed specifically for HIC in order to account for such phenomena as the salt effect [12,13].

In this study, we employed an adsorption isotherm based on colloidal energetics. It can be written as [14]

$$c^* = \frac{q^*}{K_{eq}} \exp\left[(\alpha\sqrt{q^*} + \beta)\exp\left(\frac{\omega}{q^*}\right)\right] \quad (1)$$

where c^* and q^* are the free and adsorbed protein concentrations respectively at equilibrium, and K_{eq} is the adsorption equilibrium constant. The parameters α, β and ω control the "softness" of the transition from the linear region to the plateau, and are used independently of the physical basis of the isotherm to fit the functional form to relate c^* and q^* for our experimental data.

2.2. Batch uptake

Several models have been developed to characterize protein transport in chromatographic systems. They include pore diffusion, homogeneous diffusion, surface diffusion and parallel diffusion. The latter two can be considered variants or combinations of the others, so in this study we employed the pore diffusion and homogeneous diffusion models as limiting cases to compare protein transport behavior in adsorbents with different physical properties. The theory used to estimate the effective pore diffusivity, D_p, and homogeneous diffusivity, D_h, from batch uptake data has been summarized by Chang and Lenhoff [15]. The external mass transfer coefficient, k_f, was treated as a constant during uptake and was calculated based on the correlation of Armenante and Kirwan [16]. Since the adsorption isotherm is non-linear, the batch uptake governing equations were solved numerically using IMSL (International Mathematical and Statistical Libraries) routines.

2.3. Breakthrough curve

Breakthrough (frontal elution) experiments have been widely used to evaluate ion-exchangers [17–20], affinity adsorbents [21–24], perfusion adsorbents [25] and HIC adsorbents [5] in column mode. They are particularly valuable in that this mode of operation is similar to that used in column loading in industrial practice, especially for capture steps.

The mass balance for column chromatography is written as

$$\frac{\partial c_m}{\partial t} + u\frac{\partial c_m}{\partial z} - D_L\frac{\partial^2 c_m}{\partial z^2} = -\frac{(1-\varepsilon)}{\varepsilon}\frac{\partial q}{\partial t} \quad (2)$$

where D_L is the axial dispersion coefficient, c_m is the mobile phase protein concentration, q is the protein concentration in the adsorbed phase, u is the mobile phase interstitial velocity and z is the axial position in the column. The extraparticle porosities, ε, in packed columns of the adsorbents used here were measured by inverse size exclusion chromatography [26] and are presented in Table 1. The term on the right-hand side accounts for uptake into the stationary phase, which is assumed to be governed by an appropriate transport model. The most widely used such models are the pore diffusion model, which assumes that only free protein in the pore space is able to diffuse, and the homogeneous diffusion model, in which all intraparticle protein (free or adsorbed) is able to diffuse. Detailed equations for these cases are available elsewhere [27].

Since column breakthrough experiments are usually performed in the non-linear region of the isotherm, Eq. (2) is generally solved numerically with the appropriate boundary and initial conditions. However, analytical solutions have been obtained in limiting cases of practical interest with the axial dispersion term neglected. Since our emphasis is on describing breakthrough behavior rather than a detailed mechanistic analysis, we focus on such analytical solutions. While they all incorporate some idealization, the location of the breakthrough front is determined largely by the static capacity and hence by the adsorbed concentration in equilibrium with the feed concentration. Therefore these models should all predict similar locations for the breakthrough front despite the different idealizations on which they are based.

Analytical solutions for the pore diffusion model exist for systems with rectangular adsorption isotherms [28–30]. For this limiting case, the analytical solution for the pore diffusion model used to analyze the breakthrough curves in this work is that of Cooper and Liberman, which relaxed the constant pattern assumption used previously [29].

Analytical solutions for the homogeneous diffusion model have also been developed for adsorbents with rectangular isotherms [30–32]. In this study, the experimental results were compared to the constant pattern solution of Yoshida et al., although a solution independent of the constant pattern assumption is also available

[32]. The Yoshida et al. solutions were developed by assuming that the protein concentration in the fluid phase at the surface of the adsorbent is zero until the outer surface of the adsorbent particle is completely saturated. In addition to the Yoshida et al. solution, another constant pattern analytical solution, due to Vermeulen, is also available for a quadratic driving force approximation [33,34]. This analytical solution assumes that solute adsorption can be described by the Langmuir isotherm and that there is a transition from external mass transfer control to intraparticle diffusion control during column breakthrough, and that the protein uptake rate, can be found by a lumped approximation of the solution for an intraparticle diffusion model. A simpler variant of the quadratic driving force approximation, namely a linear driving force approximation, yields yet another approximation [34].

The linear driving force approximation has been used to derive the Yoshida et al. solutions [32] as well as an analytical solution for ion-exchange and dye-affinity chromatography [35]. These solutions are in good agreement with experimental results [17,35,36], indicating that the linear driving force approximation is adequate in these two modes of chromatography.

The most appropriate approach to making direct comparisons between the Vermeulen and Yoshida solutions would be to use the Vermeulen solution with the linear driving force approximation, but this should also be modified to consider the contribution of external mass transfer, which can be the dominant mass transfer resistance at low liquid-phase protein concentrations [37]. Neglecting the external mass transfer effect can result in incorrect prediction of the early stages of column breakthrough and hence of dynamic capacity, which is an important parameter for process scale-up and design. We therefore also derived a solution for the linear driving force approximation with the consideration of external mass transfer by following the procedures of Vermeulen [34]. With the linear driving force assumption and the constant pattern conditions (i.e., $X = Y$), the rate of external mass transfer can be equated to the rate of intraparticle protein diffusion by

$$\frac{3k_f}{R}(X - X^*) = \frac{D_h\pi^2}{R^2}\Omega(Y^* - X) \tag{3}$$

where

$$X^* = \frac{c^*}{c_f} \tag{4}$$

$$X = \frac{c}{c_f} \tag{5}$$

$$Y^* = \frac{q^*}{q_s} \tag{6}$$

$$Y = \frac{q}{q_s} \tag{7}$$

In Eqs. (4)–(7), c is the solution phase concentration, c_f is the protein feed concentration, q is the protein concentration in the adsorbent, and q_s is the adsorbent binding capacity. The asterisk denotes the equilibrium value. By following the same procedures as Vermeulen [34], the dimensionless protein concentration, X_{FP}, in the mobile phase at which the transition between external mass transfer and intraparticle diffusion control takes place is found to be

$$X_{FP} = \frac{D_h\pi^2\Omega}{3Rk_f + D_h\pi^2\Omega} \tag{8}$$

and

$$\Omega = \frac{q_s}{c_f} \tag{9}$$

From $X = X_o$ to $X = X_{FP}$, the breakthrough curve is given by

$$X = \exp[\theta_F - (\theta_F)_c] \tag{10}$$

and from $X = X_{FP}$ to $X = 1$,

$$X = 1 - \exp[-\theta_P + (\theta_P)_c] \tag{11}$$

where

$$\theta_F = \frac{3k_f}{R}\frac{c_f}{q_s}\left(t - \frac{L}{u}\right) \tag{12}$$

$$\theta_P = \frac{D_h\pi^2}{R^2}\left(t - \frac{L}{u}\right) \tag{13}$$

where L is the column length, u is the mobile phase interstitial velocity and X_o is the protein concentration in the effluent when $t = L/u$. The constants $(\theta_F)_c$ and $(\theta_P)_c$ in Eqs. (10) and (11) can be computed from the transition from external mass transfer to intraparticle protein diffusion control. Here the solution capacity factor, defined in Eq. (12), for external mass transfer control at the transition, $(\theta_F)_{FP}$, is expressed as

$$(\theta_F)_{FP} = \Sigma_F + X_{FP} - \frac{3k_fR}{D_h\pi^2}\frac{c_f}{q_s}(1 - X_{FP}) \tag{14}$$

where

$$\Sigma_F = \frac{3k_f}{R}\frac{L}{u} \tag{15}$$

The solution capacity factor for intraparticle diffusion control, $(\theta_p)_{FP}$, defined in Eq. (13), at the transition, can then be found from Eqs. (12) and (13)

$$\frac{(\theta_F)_{FP}}{(\theta_P)_{FP}} = \frac{3k_fR}{D_h\pi^2}\frac{c_f}{q_s} \tag{16}$$

Once $(\theta_F)_{FP}$ and $(\theta_F)_{FP}$ are found, $(\theta_F)_c$ and $(\theta_P)_c$ can be computed from Eqs. (10) and (11) by setting X to X_{FP}. In this analytical solution, a constant pattern breakthrough curve is obtained when $\Sigma \geq 4$ and the column capacity parameter, Σ, is defined as [34]

$$\Sigma = \frac{\pi^2D_h}{R^2}\frac{q_s}{c_f}\frac{L}{u} \tag{17}$$

The k_f used in the breakthrough curve analysis was estimated from the Carberry correlation [38].

3. Materials and methods

3.1. Phenyl adsorbents and proteins

Eight phenyl stationary phases were selected for this study. The protein-accessible intraparticle porosities [18] and other physical properties of these media are summarized in Table 1. TSK-gel Phenyl-5PW and Toyopearl Phenyl 650S were purchased from Tosoh Biosep (Montgomeryville, PA, USA). All phenyl Sepharose media as well as Source 15PHE were purchased from GE Healthcare (Piscataway, NJ, USA). Fractogel EMD Phenyl (S) was obtained from EM Industries (US associate of E. Merck, Darmstadt, Germany). POROS 20 HP2 was purchased from Applied Biosystems (Foster City, CA, USA).

Four globular proteins were used as model proteins. BSA monomer (BSA), calcium-depleted bovine α-lactalbumin (ALC), hen egg white lysozyme (LYS) and hen egg white ovalbumin (OVA) were purchased from Sigma (St. Louis, MO, USA). All proteins were used without further purification. The physical properties of these proteins are shown in Table 2.

3.2. Protein solution preparation

Proteins were dissolved in 10 mM sodium phosphate, pH 7, buffer to prepare 40–50 mg/mL stock solutions. The stock solutions were then diluted to 20–25 mg/mL in 1.5 or 2 molal ammonium

Table 2
The molecular weights, MW, extinction coefficients, ε_{280}, at 280 nm, viscosity radii, R_η, adiabatic compressibilities, β, dimensions, calculated surface coverages, Γ_{cal}, and diffusivities in free solutions, D_m, of proteins used.

Protein	MW (kDa)	ε_{280} (mL/mg cm)	R_η (nm)	β ($\times 10^{-6}$ cm^3/g/bar)	Dimensions (nm^3)	Γ_{cal} (mg/m^2)	D_m (10^{-7} cm^2/s)
LYS	14.3	2.7	1.85	3.6	$4.5 \times 3.0 \times 3.0$	1.8–3.4	11.8
ALC	14.3	2.1	2.02	4.6	$3.7 \times 3.2 \times 2.5$	2.6–4.8	10.6
OVA	46	0.70	2.83	6.4	$7.0 \times 4.5 \times 5.0$	2.3–4.6	7.76
BSA	68	0.65	3.62	6.5	$14.0 \times 4.0 \times 4.0$	2.0–8.7	5.93

sulfate (AS) concentrations using 10 mM sodium phosphate containing 4 m AS and 10 mM phosphate buffers. After adjustment to pH 7 with 1 N sodium hydroxide, the protein solutions were filtered through 0.22 μm filters.

For ALC, a white precipitate formed when the protein solution was adjusted to 2 m AS. The precipitate was removed by centrifugation at 3000 g, and the supernatant was then filtered through a 0.22 μm filter. The precipitate was likely formed by non-protein impurities at high AS concentration because the removal of the precipitate did not affect the solution protein concentration. In some experiments, 1 M $CaCl_2$ solution was added to the ALC solutions to obtain a final Ca^{2+} concentration of 10 mM prior to the filtration step, as a means to stabilize ALC conformationally.

3.3. Batch uptake and adsorption isotherm measurement

The batch uptake experiments were performed in a 100 mL glass beaker in which the protein concentration was monitored continuously by recirculating the supernatant through a Rainin Dynamax UV detector (Rainin Instruments, Woburn, MA, USA) operated at 280 nm or 254 nm. Calibration curves were generated to correlate the UV absorbance and protein concentration. The recirculation loop holdup volume was 2 mL, which corresponded to a recirculation time of 10 s at a flow rate of 12 mL/min. A filter with 10 μm pores was used to prevent adsorbent particles from entering the recirculation pump and the UV detector. Agitation was provided by a 3.5 cm polypropylene 3-bladed marine-type impeller driven by an overhead electric motor at 300 rpm. The impeller was placed just below the 10 μm filter to prevent adsorbent accumulation on the filter due to the high recirculation rate. In this experimental configuration, no vortex was observed on the liquid surface.

For each experiment, a volume of 20–25 mg/mL protein stock at the appropriate AS concentration (1.5 m or 2 m) was charged into the batch uptake vessel containing a predetermined volume of AS (1.5 m or 2 m), 10 mM phosphate, pH 7, buffer to a total final volume of 61 mL. Once a steady absorbance was attained, 1 mL of protein solution was withdrawn from the vessel and the initial protein concentration of the experiment was measured by absorbance at 280 nm using the extinction coefficients [39] listed in Table 2. A predetermined volume of adsorbent slurry, equilibrated with the appropriate buffer, was transferred into a glass HPLC column and the interstitial liquid was removed by a syringe. The adsorbent was then charged into the batch uptake vessel. Under the experimental agitation conditions, the adsorbent was dispersed almost immediately once it was in contact with the protein solution. The adsorbent volume used for each experiment was 1 mL, excluding the interstitial volume. The equivalent packed bed porosities were determined previously [26].

To avoid possible adsorbent breakage due to agitation, the batch uptake experiments were terminated after 3 h, although most experiments reached steady state within 1 h. Before the agitation was stopped, 2 mL of the protein solution-adsorbent slurry was withdrawn from the vessel. After the adsorbent particles were removed by centrifugation, the protein concentration in the supernatant was measured. Another 5 mL of the slurry was also removed from the vessel into a 5 mL cryovial. This slurry was allowed to equilibrate at room temperature for an additional 12–18 h, but further changes in protein concentration in the liquid phase were usually insignificant. The amount of protein taken up by the adsorbent was calculated by mass balance, and these results were used to generate the adsorption isotherms.

For protein concentrations other than those used in the batch uptake experiments, different amounts of adsorbent slurry were dosed into predetermined volumes of protein solution. After equilibration at room temperature for 18–24 h with agitation by end-over-end rotation, the adsorbent was removed by centrifugation and the protein concentration in the supernatant was determined from the absorbance at 280 nm. For some protein concentrations, the experiments were performed in triplicate and the results were found to be highly reproducible.

3.4. Column breakthrough

AP minicolumns of 0.5 cm ID were purchased from Waters Corporation (Milford, MA, USA). Columns were flow packed to a bed height of 2.5 cm with 2 m AS in 10 mM phosphate, pH 7, buffer. In each breakthrough experiment, the freshly packed column was equilibrated with the appropriate buffer before the protein solution was loaded. Column packing and breakthrough experiments were performed at different flow rates of 2 m AS in 10 mM phosphate buffer, pH 7, using an Äkta Explorer HPLC (GE Healthcare, Piscataway, NJ, USA). Protein concentrations were in the range 0.9–1.0 mg/mL. The column back-pressure was maintained at 0.2–0.3 MPa with a flow restrictor to prevent channeling.

4. Results and discussion

4.1. Adsorption isotherms and dynamic capacity

The adsorption isotherms of proteins on different phenyl media are depicted in Fig. 1. Well-defined plateaus are not present in any of the cases, as is typical for HIC media and is consistent with the results of Chen and Sun [12] and Xia et al. [13]. Comparison of the adsorption isotherms of the same protein on different media shows Sepharose FF HS and POROS 20 HP2 to have the highest and lowest capacities, respectively. Sepharose FF LS and Sepharose HP have similar capacities, which is consistent with their similar ligand densities and protein-accessible surface areas per unit media volume (Table 1), although their pore size distributions (PSDs) are different [26]. Sepharose FF HS and Sepharose FF LS have identical PSDs [26] but the ligand density of the former adsorbent is twice that of the latter. At 2 m AS, the capacities of Sepharose FF LS for LYS and OVA are approximately 90% those of Sepharose FF HS. These results suggest that the capacities of the Sepharose adsorbents are largely controlled by the phase ratios, but not the PSDs or ligand densities of the media.

Comparing the adsorption isotherms of different proteins on the same adsorbent shows the capacities for LYS to be higher than those of OVA in the agarose and polymethacrylate media (Fig. 1A, B, D and E). However, the capacities of these two proteins on the polystyrene divinybenzene (PS-DVB) media are essentially the same (Fig. 1F).

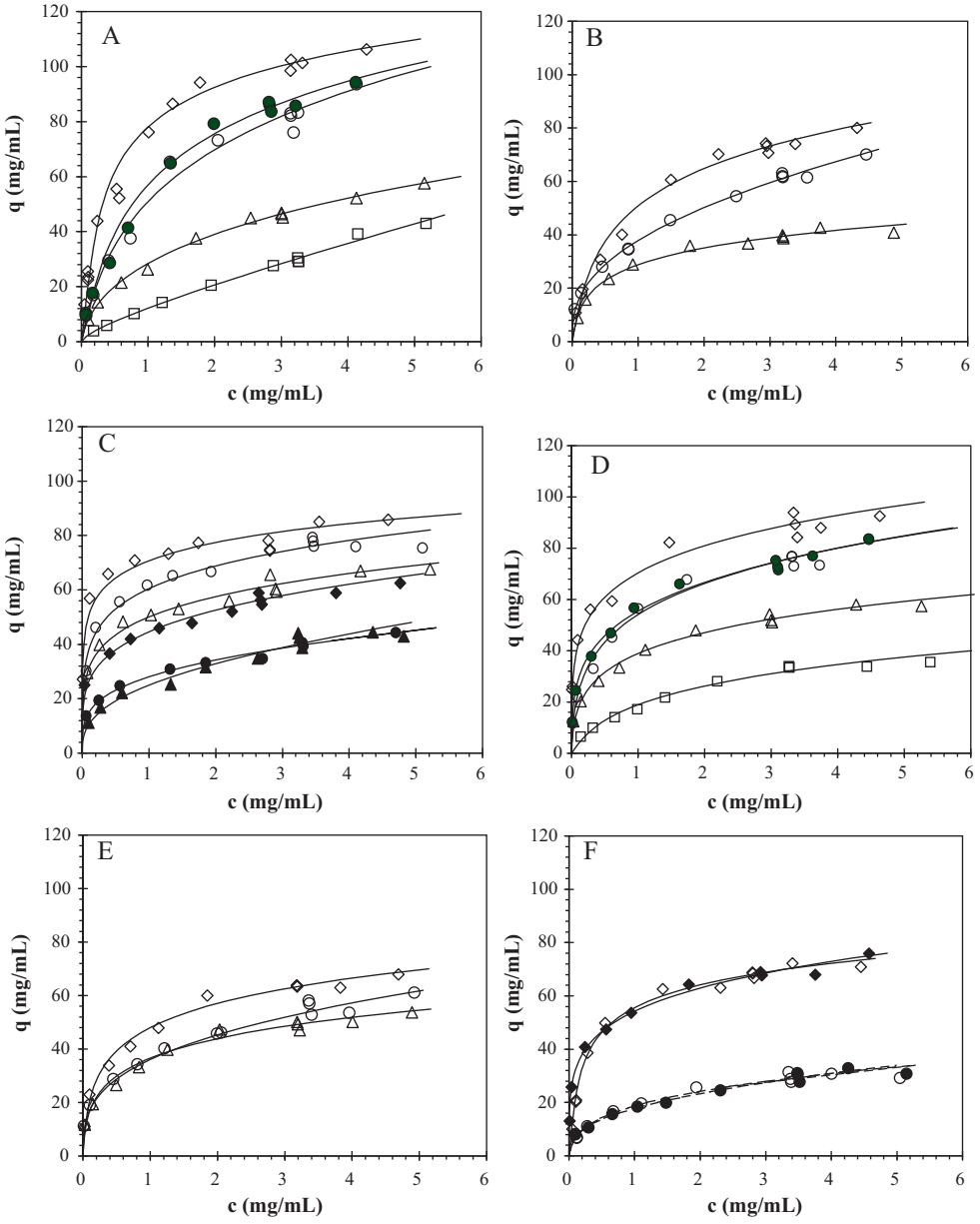

Fig. 1. Adsorption isotherms of proteins on phenyl media. (A) LYS on agarose phenyl media: FFHS, 2 m AS (◊); FFLS, 2 m AS (○); HP, 2 m AS (●); FFHS, 1.5 m AS (△); FFLS, 1.5 m AS (□). (B) LYS on polymethacrylate phenyl media: Toyopearl 650S, 2 m AS (◊); Fractogel EMD S, 2 m AS (○); TSK-gel 5PW, 2 m AS (△). (C) ALC and BSA on phenyl Sepharose FF HS media. BSA, 2 m AS (◊); BSA, 1.5 m AS (♦); ALC, 2 m AS (○); ALC, 1.5 m AS (●); ALC, 2 m AS + 10 mM Ca^{2+} (△); ALC, 1.5 m AS + 10 mM Ca^{2+} (▲). (D and E) OVA on agarose and polymethacrylate phenyl media. Symbols as in A and B, respectively. (F) LYS and OVA on polystyrene-divinylbenzene media. LYS and Source (◊); OVA and Source (♦); LYS and POROS (○); OVA and POROS (●).

Table 3 summarizes the fitting parameters and initial slope, S, of the adsorption isotherms, as well as the capacities and surface protein concentrations at $c^* = 4$ mg/mL. The initial slopes of the isotherms can be used to reflect protein affinities for the adsorbents. In fact, the retention factor, k', of an isocratic elution can be calculated from S based on [40]

$$k' = \frac{FS}{1 + F\varepsilon_P} \tag{18}$$

$$F = \frac{1-\varepsilon}{\varepsilon} \tag{19}$$

For example, k' of LYS on Sepharose FF LS at 1.5 m ammonium sulfate calculated from Eq. (18) is 15, which agrees reasonably well with the result obtained from isocratic elution ($k' = 21$).

From Eq. (1), K_{eq} should reduce to S at low protein concentration, c^*, and indeed S and K_{eq} are similar in numerous cases. However, in other cases, the two quantities differ significantly. The most likely reason for this is that K_{eq} is estimated by a global fit of Eq. (1) to experimental isotherm data, with all four parameters retained in order to obtain the best description of the curve rather than any particular mechanistic insights. Therefore deviations between S and K_{eq} could be due to correlations among parameters coupled with scatter in the data.

Table 3 shows that S decreases with decreasing AS concentration, and that the S values of proteins on the same adsorbent follow the order BSA > OVA > ALC > ALC + Ca^{2+} > LYS, consistent with the results obtained from isocratic elution [26]. The results in Table 3 also suggest that there is no clear correlation between protein affinity and adsorbent capacity. However, there is a clear trend that adsorbents with higher accessible surface areas (shown in Table 1) also have higher capacities.

Table 3
Fitting parameters and initial slope, S, of adsorption isotherms, binding capacities, q, and surface protein concentrations, Γ, of HIC media at $C^* = 4$ mg/mL.

Media	[AS] (m)	S	K_{eq}	α	β	ω	q (mg/mL)	Γ (mg/m^2)
LYS								
FFHS	2	308	205	7.8	0.0	−37.7	106	1.8
FFLS	2	132	105	0.6	0.0	−13.0	92	1.7
HP	2	158	103	1.5	0.8	−22.7	94	1.9
Toyopearl	2	194	127	1.5	0.0	−17.3	79	3.1
TSK	2	103	151	1.8	0.0	−9.4	42	3.1
Fractogel	2	289	9200	0.0	9.5	−3.4	65	2.4
Source	2	202	239	7.0	0.0	−26.7	72	2.8
POROS	2	59	118	0.0	10.8	−7.7	30	3.7
FFHS	1.5	80	198	0.4	0.0	−0.7	52	0.9
FFLS	1.5	22	71	0.0	2.6	−1.4	37	0.7
OVA								
FFHS	2	4140	13,389	0.2	19.8	−11.8	91	1.8
FFLS	2	728	1104	0.7	0.1	−3.8	80	1.6
HP	2	1545	3494	0.0	15.3	−9.7	81	1.9
Toyopearl	2	425	338	1.7	0.2	−12.5	66	2.8
TSK	2	436	523	1.2	0.0	−5.8	52	4.1
Fractogel	2	660	5214	0.0	11.4	−5.0	52	2.4
Source	2	1302	19,818	0.0	20.2	−9.1	73	3.1
POROS	2	82	2444	0.0	9.3	−2.7	30	3.9
FFHS	1.5	400	716	0.9	0.1	−4.5	56	1.1
FFLS	1.5	46	38	0.9	0.4	−8.2	33	0.7
ALC								
FFHS	2	540	19,365	0.0	25.6	−11.6	74	1.4
FFHS	1.5	233	327,906	0.0	16.1	−2.9	41	0.8
FFHS	2 + Ca^{2+}	388	63,798	0.0	21.8	−7.9	65	1.2
FFHS	1.5 + Ca^{2+}	117	9845	0.0	10.1	−2.6	42	0.8
BSA								
FFHS	2	5436	420,776	1.7	4.5	−6.3	85	1.9
FFHS	1.5	715	886,018	0.0	19.2	−4.4	60	1.4

The surface protein concentrations, Γ, were calculated by dividing the capacities by the phase ratios and are shown in Table 3. The Γ values on the agarose media are consistently lower than those on the polymethacrylate and PS-DVB adsorbents despite the fact that the agarose media have the highest capacities. This may be because the accessible surface areas of the adsorbents were calculated by assuming that the media comprise cylindrical pores, which is certainly a simplification of the actual pore structures of the adsorbents. This is especially true for the gel-like structure of the agarose media, and would affect the values of Γ. For close-packed arrangements, the monolayer surface coverages of proteins can be estimated from their dimensions [41–43] and are summarized in Table 2, where the ranges presented account for the possible orientations of the adsorbed proteins (side-on or end-on). These calculated values, Γ_{cal}, show that the experimental values of Γ in Table 3 are consistent with monolayer coverage or less. The coverages at 1.5 m are appreciably below monolayer values, presumably reflecting the relatively low protein-surface affinity. The capacities at 2 m AS are, as expected, closer to monolayer coverage, with those for LYS and OVA within or just below the calculated range for all the adsorbents studied. The results for ALC and BSA include fewer adsorbents. The coverage of ALC here is distinctly below the monolayer ranges even at 2 m AS. Because BSA is generally assumed to be a highly elongated ellipsoid, its Γ_{cal} range is wide. The experimental results shown in Table 3 may reflect side-on adsorption, consistent with the orientation of adsorbed BSA on PS-DVB inferred from atomic force microscopy observations [42]. However, the assumption of ellipsoidal BSA may not be accurate because the related molecule, human serum albumin (HSA), is heart-shaped and can be approximated as a solid equilateral triangle with sides of approximately 8 nm [44]. With this shape, the close-packed monolayer surface coverage of BSA is estimated to be 4.1 mg/m^2, which is significantly higher than the experimental results shown in Table 3.

Protein conformational changes could also affect the capacity. More flexible proteins have a higher degree of conformational change when adsorbed on HIC surfaces [45,46], and if this leads to more extensive spreading it would result in a lower capacity. However, such considerations are not always straightforward, with the results for ALC instructive in this regard. The capacity of ALC on Sepharose FF HS is lower than that of LYS although the two proteins have similar MW. This could be due in part to different adsorption orientations, but the ALC is also much more susceptible to conformational change in HIC. The presence of 10 mM Ca^{2+}, intended to increase the conformational stability of ALC, decreases the capacity of Sepharose HS for ALC (Fig. 2C). This is unexpected because a more stable tertiary structure should give rise to less conformational change and spreading and therefore, if anything,

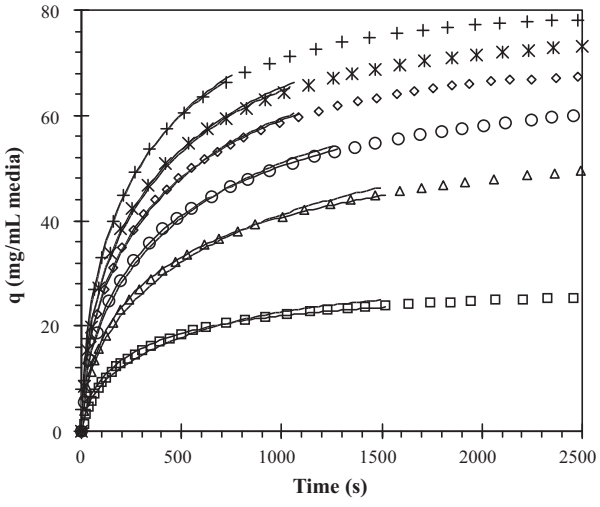

Fig. 2. Comparisons of calculated (lines) and experimental (symbols) BSA uptake on phenyl Sepharose FF HS in 2 m AS, pH 7 buffer. Solid line: pore diffusion model; dotted line: homogeneous diffusion model. Initial bulk protein concentrations (from top): 3.03, 2.51, 1.97, 1.48, 1.06, 0.46 mg/mL.

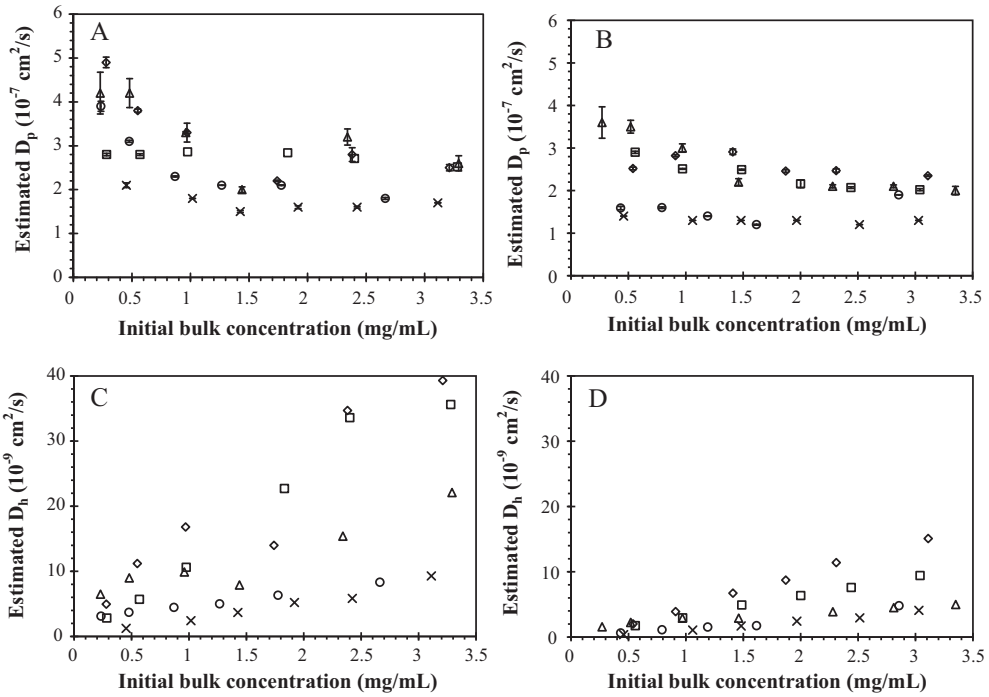

Fig. 3. Effective protein diffusivities in Sepharose FF HS estimated by the pore diffusion model (A, B) and homogeneous diffusion model (C, D) as a function of initial bulk concentrations in 1.5 m AS, pH 7 buffer (A, C) and 2 m AS, pH 7 buffer (B, D). The error bars shown in A and B are the uncertainties of the least squares fits with 95% confidence interval. LYS (△); ALC (□); ALC with Ca^{2+} (◊); OVA (○); BSA (×).

increased capacity. However, ALC has a weaker affinity for agarose HIC adsorbents in the presence of Ca^{2+} [26], and this should offset the increased capacity expected from a reduction of spreading. In addition, ALC unfolding can occur in HIC even in the presence of Ca^{2+} [47].

4.2. Batch uptake

Batch uptake experiments were performed with four proteins and eight phenyl adsorbents on different base matrices. The intraparticle protein diffusivities were estimated from all data sets

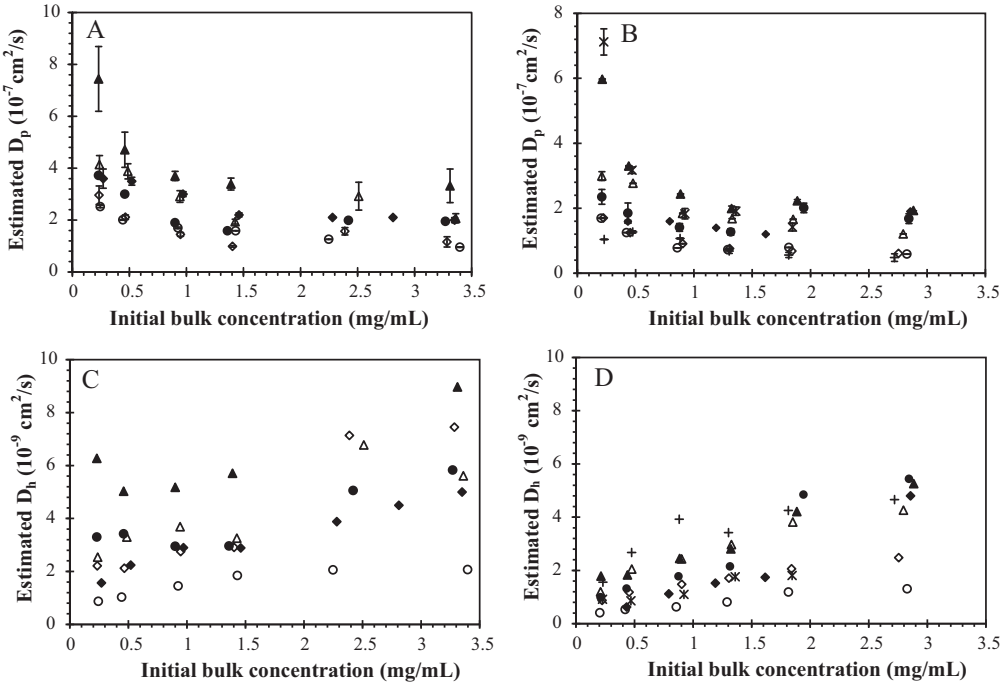

Fig. 4. Effective diffusivities of LYS (A, C) and OVA (B, D) in HIC media estimated by the pore diffusion model (A, B) and homogeneous diffusion model (C, D) as a function of initial bulk concentrations in 2 m AS, pH 7 buffer. The error bars in A and B represent the uncertainties of the estimated diffusivities with 95% confidence interval. Sepharose HP (▲); Sepharose FF HS (♦); Sepharose FF LS (●); Toyopearl 650S (△); TSK 5PW (◊); Fractogel EMD (○); Source (*); POROS (+).

for both the pore diffusion and homogeneous diffusion models. Fig. 2 depicts the uptake of BSA in Sepharose FF HS in 2 m AS. The experiments were continued until the changes in the supernatant protein concentration became insignificant. The uptake was fast, and largely complete within 30 min, although additional slow uptake persisted over a long period of time but with relatively little additional protein accumulating. Other uptake systems showed similar trends but with even faster uptake rates.

The data fits emphasized the range over which most of the uptake (70–80%) took place, since this is the region of greatest interest in column experiments. The adsorbents were treated as being monodisperse, with mean diameters as listed in Table 1. Chang and Lenhoff [15] and Carta and Ubiera [48] incorporated the particle size distribution into diffusivity estimation, but the differences were marginal and at the expense of longer computation times. Fig. 2 also shows the calculated fits for BSA uptake in Sepharose FF HS. Both models fit the experimental data equally well. Similar results were observed in other uptake systems. Therefore, the governing protein transport mechanism cannot be determined simply by fitting experimental data to the diffusion models. The only systems for which good fits could not be obtained were LYS in Source and POROS media. The uptake of LYS in these two media was complete in less than 30 s, and under such conditions, experimental errors due to the adsorbent dispersion time and the time delay in data recording due to the recirculation loop holdup volume could become significant. Therefore, LYS diffusivities in these two media are not presented.

The effect of the initial bulk concentration on protein diffusivities in Sepharose FF HS is depicted in Fig. 3. The error bars shown in Fig. 3A and B represent the standard errors of the estimated pore diffusivities, D_p, with 95% confidence level [49]. The small confidence intervals indicate that the calculated uptake profiles are in good agreement with the experimental results. There is a consistent trend that the D_p values decrease with increasing initial bulk protein concentration, and this trend is statistically significant. The D_p values of LYS and ALC are similar, as is expected because these proteins have similar molecular sizes, viscosity radii and dimensions. The addition of Ca^{2+} does not have a significant effect on the D_p of ALC although it stabilizes ALC's tertiary structure and reduces the affinity of ALC for HIC media. OVA and BSA are larger proteins than LYS and ALC and have concomitantly smaller D_p values.

Fig. 3C and D show that the homogeneous diffusivities, D_h, of proteins in Sepharose FF HS increase roughly linearly with increasing initial bulk concentration. This trend is opposite to what is observed for D_p. In addition, the D_h of LYS and ALC are different although they have similar molecular masses.

Fig. 3 also shows that both D_p and D_h increase with decreasing salt concentration, a trend opposite to that found in ion-exchange adsorbents [15]. Since the dependence of adsorption on salt concentration is opposite in these two systems, the results may indicate that the coupling of protein adsorption and transport is not completely accounted for by the model equations. An alternative explanation is that adsorption actually changes the effective transport rate, perhaps by reducing the effective pore size for diffusion. It has been shown that adsorbed polymers can reduce the effective pore volume of silica gel [9]. Both theoretical calculations [50] and experimental results [51] show that electrostatic repulsion between charged proteins and the pore walls reduces protein partitioning into porous media. Therefore, protein-adsorbent pore wall repulsion and potentially protein–protein repulsion could also retard protein diffusion in the pore space. This could be significant especially in ion-exchange, where low ionic strengths are usually employed, but is less likely at the high salt concentrations used in HIC.

The diffusivities of LYS and OVA in different phenyl media are summarized in Fig. 4. There is a consistent trend that the pore diffusivities of these two proteins decrease with increasing initial bulk protein concentration in all of the adsorbents used for this study. This is consistent with the results shown in Fig. 3 as well as with the results of Chang and Lenhoff [15]. Statistical analysis shows that the differences in pore diffusivities among these adsorbents are significant based on 95% confidence intervals. The homogeneous diffusivities increase with increasing initial bulk concentration, consistent with those shown in Fig. 3C and D. The relation between pore and homogeneous diffusivities is discussed later.

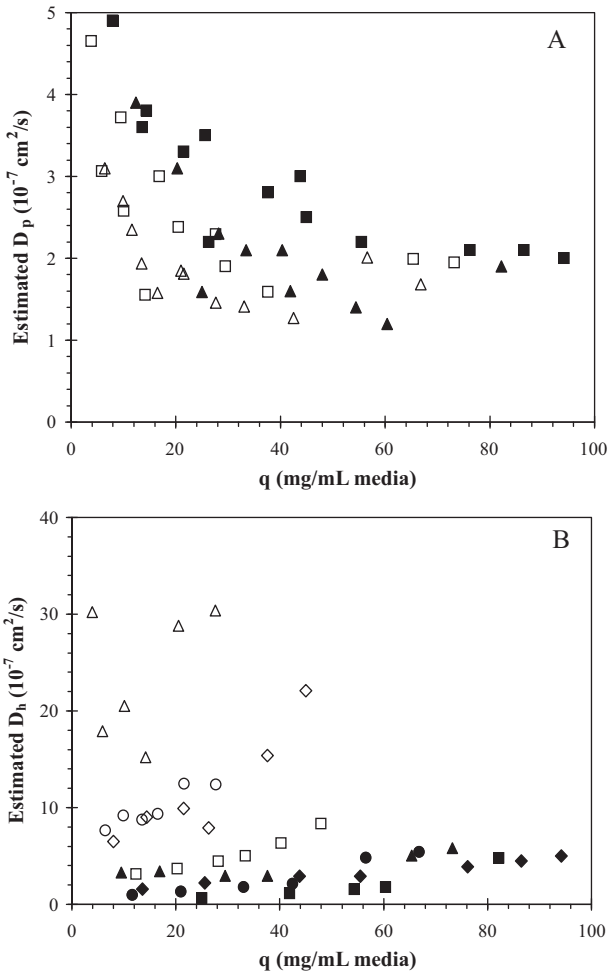

Fig. 5. The effect of protein loading, q, on the effective diffusivities of LYS and OVA in Sepharose FF media estimated by the pore diffusion model (A) and the homogeneous diffusion model (B). (A) LYS_HS (■); LYS_LS (□); OVA_HS (▲); OVA_LS (△). B: LYS_HS (◊); LYS_LS (△); OVA_HS (□); OVA_LS (○); 1.5 m AS (open symbols); 2 m AS (solid symbols).

The results shown in Fig. 4 do not allow direct comparison of the effect of protein loading on protein transport. The adsorbed protein could affect the diffusivity via pore constriction or steric repulsion between adsorbed and free protein. Fig. 5 provides an alternative way to analyze the effect of adsorbent properties on intraparticle protein transport. The pore diffusivities of LYS and OVA in Sepharose FF HS and Sepharose FF LS are plotted against q, the amount of protein adsorbed at equilibrium, to allow the effect of adsorbed protein on the diffusivities to be compared directly. The wide ranges of q shown were obtained by using different bulk protein concentrations at 1.5 m or 2 m AS.

Fig. 5A shows that the pore diffusivities in Sepharose FF HS are consistently higher than those in Sepharose FF LS at similar loadings, especially when the amount of protein adsorbed is below 40 mg/mL media. At higher protein loadings, the pore diffusivities in these two media are similar. The pore structure does not

contribute to the differences observed because these two agarose media have essentially identical pore structures [26]. Therefore, the diffusivity trends must be related to the only difference between the two media, namely that the ligand density of Sepharose FF HS is double that of Sepharose FF LS. Results from isocratic elution experiments show that proteins have higher affinities for HS than for LS [26], and the isotherms show higher capacities for HS than for LS, with the fractional difference highest at low concentrations (Fig. 1). Therefore equal values of q correspond to lower initial bulk concentrations on HS than on LS, especially at low concentrations, and since the pore diffusivities are based on a driving force given by the bulk concentration, the effective pore diffusivities observed in HS are higher than those in LS. When the initial bulk concentration is high, the relative amounts of protein in the liquid phases adsorbed by both HS and LS could become comparable, as reflected by the adsorption isotherms shown in Fig. 1. Therefore, the pore diffusivities become independent of both q and ligand density.

Fig. 5B shows the effect of protein loading on the homogeneous diffusivities of LYS and OVA. The D_h values increase gradually with increasing protein loading. At 2 m AS, the D_h values of both proteins in Sepharose FF HS and Sepharose FF LS are similar, indicating that the effect of ligand density on D_h is not significant. At 1.5 m AS, the D_h values of both proteins are consistently higher than those at 2 m AS. With the same ligand density, the D_h values of LYS are higher than those of OVA. For the same protein, the D_h values in Sepharose FF LS are higher than those in Sepharose FF HS. These results suggest that at the same protein loading, lower protein affinity for the adsorbent leads to higher D_h. This is consistent with the hypothesis that a strong protein-adsorbent interaction can retard protein transport if homogeneous diffusion is the protein transport mechanism. A mechanistic basis for this can be found in a parallel diffusion model [52], for which the quantitative dependence on protein binding affinity has been incorporated explicitly for ion-exchange systems [53].

In comparing protein diffusivities in materials with differences in their base matrices, the pore structures are an important factor in understanding the differences in diffusivities. The effects of pore structure on hindered diffusion can be expressed as [54]

$$D_p = \frac{\varepsilon_p \lambda}{\tau} D_m \tag{20}$$

where τ is the tortuosity of the adsorbent. The diffusion hindrance factor, λ, arises due to the hydrodynamic interaction between diffusing protein molecules and the pore walls, and can be estimated from the ratio of protein and pore radii, η, by [55]

$$\lambda \sim 1 - \frac{9}{8}\eta \ln \eta^{-1} - 1.539\eta \tag{21}$$

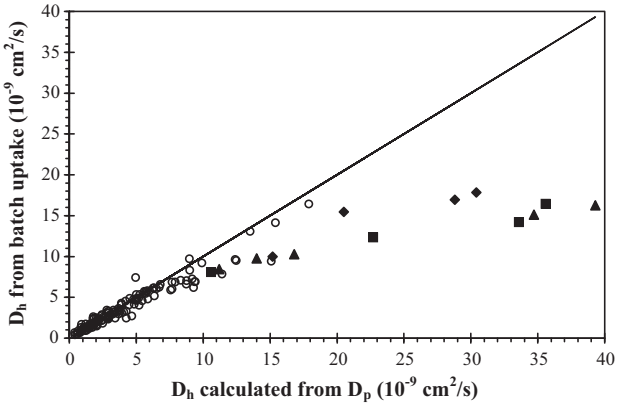

Fig. 6. Comparisons of D_h estimated from batch uptake and calculated from D_p values. ■: ALC; 1.5 m AS + 10 mM Ca^{2+}; Phenyl Sepharose FF HS. ▲: ALC; 1.5 m AS; Phenyl Sepharose FF HS. ♦: LYS; 1.5 m AS; Phenyl Sepharose FF LS. ○: All other experiments.

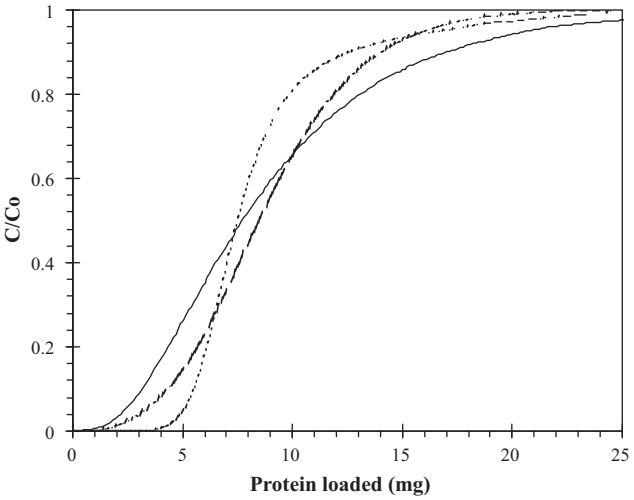

Fig. 7. The effect of feed flow rate on LYS breakthrough in phenyl Sepharose FF LS at 2 m AS, pH 7 buffer. 0.3 mL/min (dotted line); 0.6 mL/min (dashed line); 1.3 mL/min (solid line).

Among the agarose media, the pore diffusivities follow the order Sepharose HP > Sepharose FF HS ~ Sepharose FF LS (Fig. 4A and B). Sepharose FF HS and Sepharose FF LS have identical pore structures [26] but different ligand densities. It should be noted that the uptake experiments for the agarose media shown in Fig. 3 were performed with protein loadings of 40 mg/mL media or more. At high protein loadings, the higher amount of adsorbed protein in Sepharose FF HS does not have a significant effect on D_p. Sepharose HP has a similar porosity to those of the other two agarose media (Table 1), but its mean pore radius is almost 50% larger. The larger pore size reduces the diffusion hindrance, λ, hence increases the protein diffusion rate.

For the methacrylate media, the diffusivities in Toyopearl 650S are higher than those in TSK-gel 5PW (Fig. 4). Toyopearl 650S and TSK-gel 5PW have similar mean pore radii, but the much higher porosity of Toyopearl 650S may improve intraparticle protein transport, consistent with Eq. (21). The diffusivities in Fractogel EMD are similar to those in TSK-gel 5PW although the former has a smaller mean pore diameter and lower porosity. Therefore, factors other than pore size and porosity may play a role in protein transport in Fractogel EMD. Differences in pore tortuosity and connectivity may be among the reasons, as may the presence of "tentacles" in defining the "pore" structure of Fractogel EMD and in determining the nature of adsorption. Pore connectivity and tortuosity may also explain the faster protein diffusion in Source than in

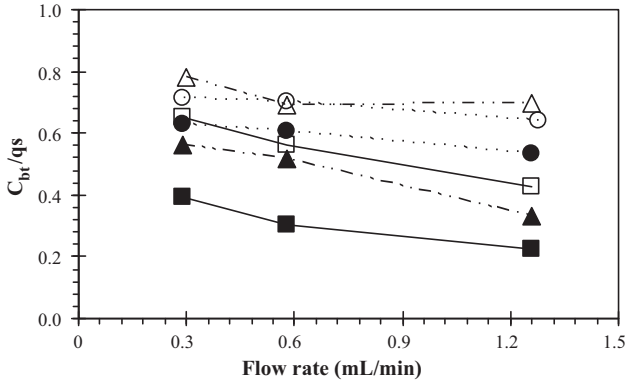

Fig. 8. The effect of feed flow rate on column capacities for LYS at 10% breakthrough. POROS (△, q_s = 18 mg/mL); Source (○, 55 mg/mL); Fractogel (□, 39 mg/mL); Toyopearl (▲, 49 mg/mL); TSK (●, 28 mg/mL); Sepharose FF LS (■, 49 mg/mL).

POROS although the former has a smaller mean pore diameter and lower porosity.

The normalized pore diffusivities, D_p/D_m, of proteins in the phenyl media are generally in the range 0.1–0.5, in good agreement with those estimated by plate height analysis [8]. From Eqs. (20) and (21), the tortuosities are estimated to be between 1 and 7, in agreement with the usual range for porous media [2]. The Biot numbers calculated from the D_p values are in the range 10–90, indicating that the overall transport process is controlled by intraparticle diffusion.

Figs. 3 and 4 show the D_p values to be consistently 1–2 orders of magnitude higher than the homogeneous diffusivities, D_h. D_p can be related approximately to D_h by [15]

$$D_h = \left(\frac{\varepsilon_p}{\varepsilon_p + (\partial q/\partial c)} \right) D_p \tag{22}$$

where $\partial q/\partial c$ is the slope of the adsorption isotherm and is a function of uptake time. A similar result was also obtained by Weaver and Carta [17]. A reasonable approximation for $\partial q/\partial c$ in Eq. (22) is q_s/c_o, where q_s is the adsorption capacity in equilibrium with the initial bulk concentration, c_o. The reasoning behind this approximation is discussed elsewhere [15]. Due to the shape of the isotherms, $\partial q/\partial c$ decreases with increasing c_o, so D_h increases with increasing c_o, consistent with the trends shown in Figs. 3 and 4.

To validate Equation 22, D_h values estimated from the pore diffusion model were plotted against corresponding values calculated from D_p (Fig. 6). The data points generally fall on or very close to the diagonal line, showing the equivalence of the two models in HIC systems. However, for higher D_h values the quantities calculated from D_p are lower than those estimated directly from the batch uptake results. These points correspond to systems with lower protein loadings (Fig. 5), and the discrepancy may simply reflect the approximations inherent in evaluating Eq. (22) in the steeper region of the isotherm rather than any significant loss of applicability of the equation itself.

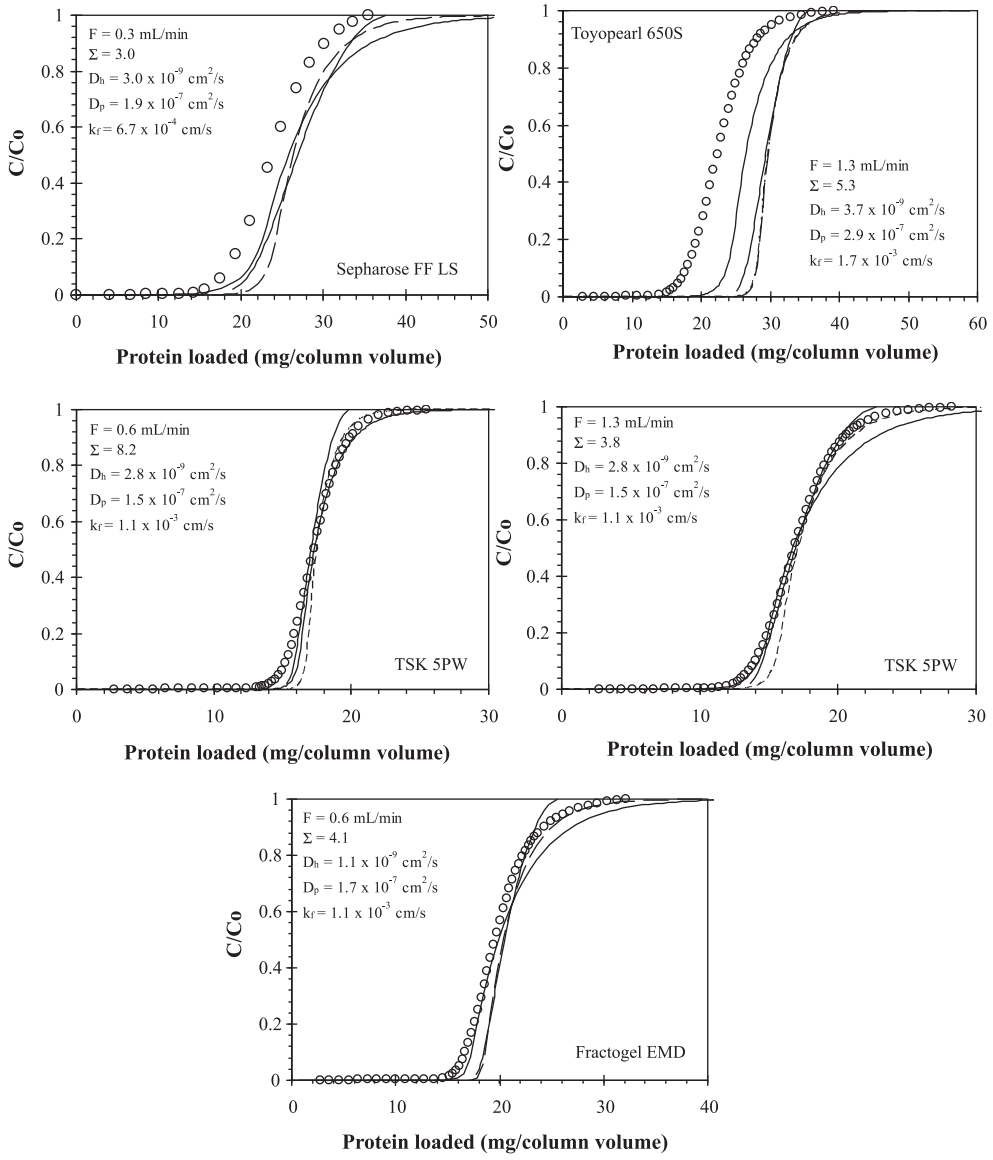

Fig. 9. Comparisons of calculated and experimental breakthrough curves of LYS in different phenyl media in 2 m AS, pH 7 buffer. Experimental data (○); homogeneous diffusion model of Vermeulen (solid line); homogeneous diffusion model for rectangular isotherm of Yoshida et al. (dashed line); pore diffusion model for rectangular isotherm (dotted line).

4.3. Column breakthrough

4.3.1. Effect of feed flow rate on shape of breakthrough curves in HIC

To evaluate the performance of the adsorbents in column mode, breakthrough experiments were performed with LYS and OVA at different mobile phase flow rates of 2 m AS in 10 mM phosphate buffer, pH 7, for protein concentrations of 0.9–1.0 mg/mL. Fig. 7 shows the breakthrough curves of LYS on Sepharose FF LS. The effect of the mobile phase flow rate on the breakthrough behavior is typical, with shallower slopes and earlier breakthrough at higher flow rates. The same trend was observed in all other systems, although the flow rate effect was less pronounced. A large set of breakthrough curves for BSA in HIC adsorbents has been reported elsewhere [7], but a detailed analysis of the breakthrough behavior was not presented. Most of our analysis is devoted to the results for LYS since these data represent the most consistent data set; concerns regarding the OVA data set are discussed in Section 4.3.3.

4.3.2. Dynamic capacities of HIC adsorbents

For preparative chromatography, the breakthrough capacity is an important parameter in process design and adsorbent selection. Fig. 8 shows the effect of feed flow rate on the 10% LYS breakthrough (dynamic binding capacity, DBC) on different phenyl adsorbents. The breakthrough capacities, C_{bt}, are normalized by the static capacities, q_s, calculated from the adsorption isotherms, to provide an indication of transport limitations; the static capacities are given in the figure captions to allow back-calculation of the actual DBCs. The column utilizations prior to 10% breakthrough range from 20% to 80% of the static capacities, depending on adsorbent type and feed flow rate. POROS 20 HP2 and Source 15PHE have the highest normalized DBC while Sepharose FF LS has the lowest; these extremes are consistent with the respective particle sizes

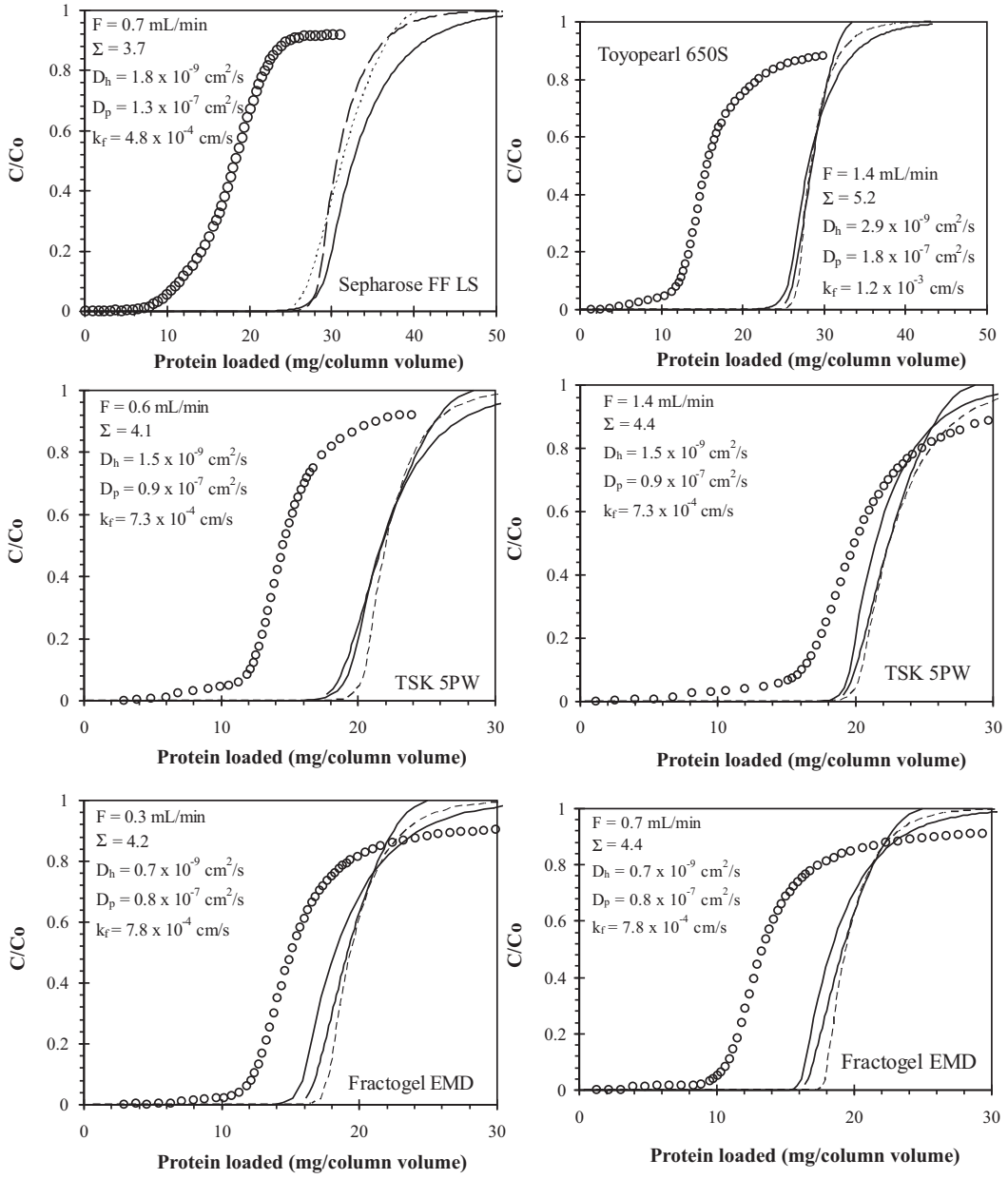

Fig. 10. Comparisons of calculated and experimental breakthrough curves of OVA in different phenyl media in 2 m AS, pH 7 buffer. Experimental data (○); homogeneous diffusion model of Vermeulen (solid line); homogeneous diffusion model for rectangular isotherm of Yoshida et al. (dashed line); pore diffusion model for rectangular isotherm (dotted line).

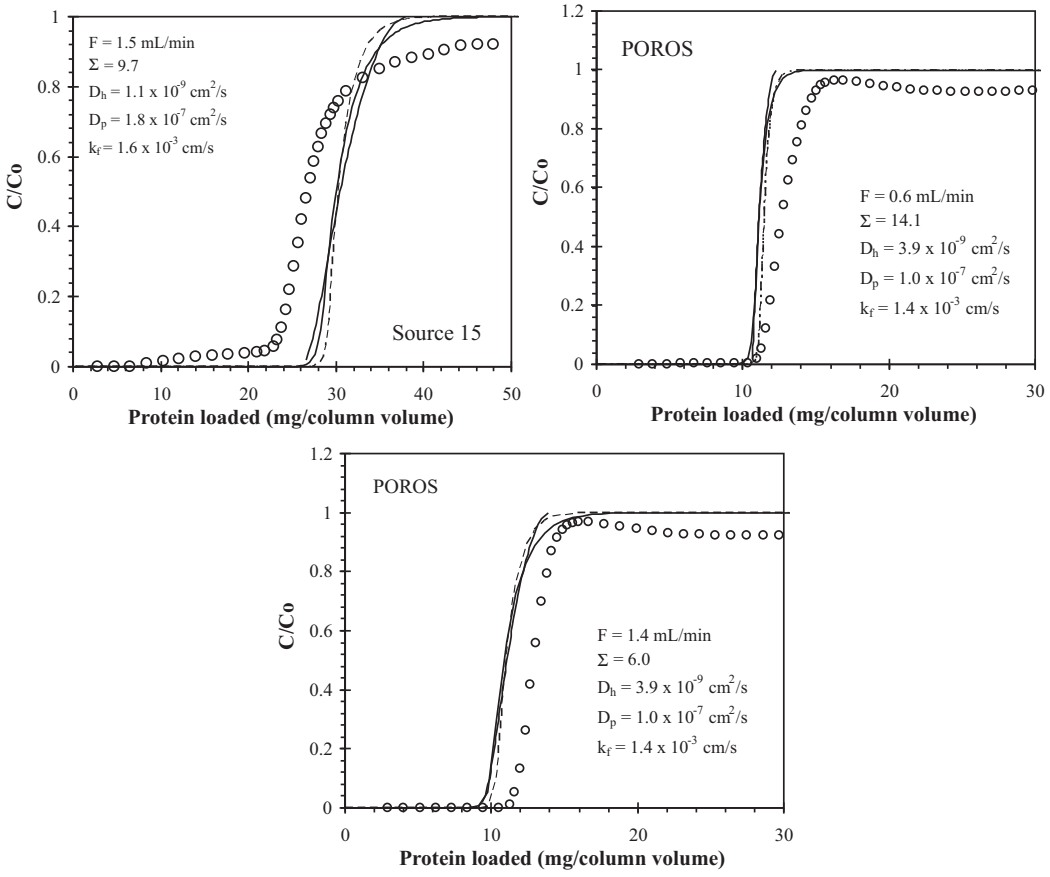

Fig. 10. (*Continued*)

(Table 1). At the same feed flow rates, TSK-5PW has a higher normalized DBC than Toyopearl 650S despite its larger particle size and the lower diffusivity than for Toyopearl 650S. A possible reason for this discrepancy is a difference in the column packing, which could result in different static capacities per unit column volume to those expected based on particle volume. Unfortunately void volumes were not measured for the columns used for these experiments. Other factors could include compression of the adsorbents and/or transport limitations due to contacts between adsorbent particles in packed columns [56,57].

4.3.3. Prediction of column breakthrough in HIC

A more detailed analysis of the breakthrough behavior requires use of the analytical equations summarized in Section 2. Analytical solutions are available for the pore diffusion model in systems with rectangular isotherms, a limiting situation that is a rather poor approximation to the experimental isotherms (Fig. 1). For pore diffusion with non-linear isotherms, Eq. (2) is usually solved numerically. For the homogeneous diffusion model, however, analytical solutions were calculated for stationary phases using the Yoshida et al. [32] and Vermeulen [34] solutions under constant pattern conditions. In these calculations, the diffusivities used were those estimated from the batch uptake experiments, the adsorbent capacities were determined from the adsorption isotherms and the external mass transfer coefficients were calculated from Carberry [38]. Therefore, no adjustable parameters were involved in the breakthrough curve calculations. Based on Eq. (17), conditions of low D_h, q_s, and/or large particle radius require a longer column to achieve constant pattern conditions. As a result, for some adsorbents used in this study, longer columns were required to reach $\Sigma \geq 4$.

Fig. 9 compares the experimental breakthrough curves of LYS with those calculated from the analytical solutions for Sepharose FF LS, Toyopearl 650S, TSK-5PW and Fractogel EMD. All three analytical solutions give similar breakthrough predictions, suggesting that the dominant transport mechanisms in HIC adsorbents cannot be distinguished by the column breakthrough method. With the exception of Toyopearl 650S, the analytical solutions are in good agreement with the experimental results. There is also a trend that the Vermeulen solution provides a better prediction for the early part of the breakthrough while the Yoshida et al. solution provides a better prediction towards the end of the breakthrough. For Toyopearl 650S, the 10% breakthrough predicted by the Vermeulen solution is 25% higher than the experimental result. The factors underlying the poorer prediction are not readily apparent.

Fig. 10 summarizes the breakthrough curves of OVA on the various adsorbents. Although the calculated breakthrough fronts are similar in form to the experimental curves, all three analytical solutions overestimate the breakthrough capacities of the adsorbents. A noteworthy observation is that, in general, C/C_o did not reach unity within the time frames of the experiments. Similar behavior was also observed with BSA in other HIC adsorbents [7] and ion-exchangers [58]. This phenomenon could be due to the presence of impurities in the protein samples [59]. To investigate this further (see Supplemental Information for details), the feed solution, fractions from the breakthrough curve, and the effluent pool were collected and analyzed. SDS-PAGE and gradient elution [60] showed that the feed contained multiple protein species in addition to OVA; based on the optical densities of the bands on the SDS-PAGE gels, the OVA content in the feed for the breakthrough experiments was estimated to be $57 \pm 8\%$, suggesting a sufficiently high level of impurities to explain the discrepancies between the calculated and measured breakthrough curves.

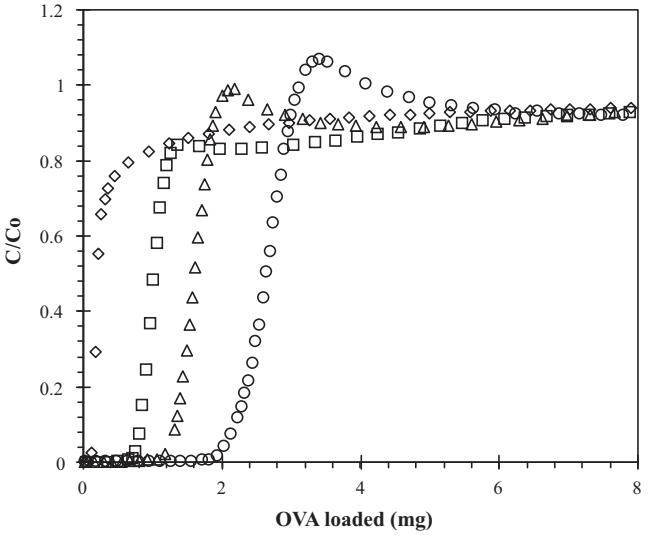

Fig. 11. Effect of AS concentration on OVA breakthrough in POROS at 1.6 mL/min. The feed protein concentration was 0.2 mg/mL. 1 m (◊); 1.5 m (□); 1.8 m (△); 2 m (○).

The behavior was more complex on the POROS 20 HP2 adsorbent than on the other adsorbents, with an overshoot preceding the region of apparently asymptotic approach to $C/C_o = 0.9$. The overshoot was found to be sensitive to the AS concentration, developing from a shoulder into the overshoot peak with increasing AS concentration (Fig. 11), indicating that it occurs at high protein-adsorbent affinity. These results suggest that the overshoot phenomenon observed could be due to competitive adsorption. Similar conclusions were drawn from ion exchange [61] and other hydrophobic interaction [62] systems. The reason that it was observed here only in the POROS media was not explored in detail, but it may be related to the lower reversibility of adsorption of proteins in general and ovalbumin in particular on polystyrene-divinylbenzene base matrices [26].

5. Conclusions

Protein adsorption isotherms on HIC resins are much softer than those on ion exchangers, indicating that the protein binding affinities are weak. The binding affinities can be increased by increasing the AS concentration and ligand density, although this may promote conformational change and irreversible adsorption. Increased binding affinity can increase the static capacity for a given protein concentration, but the maximum static capacities of phenyl resins are largely determined by the protein-accessible surface area, as is also the case for ion exchangers. Designing a novel resin with increased surface area requires reducing the pore size, which involves a delicate balancing of such issues as protein accessibility and transport rates.

Batch uptake can be used to evaluate the effects of column loading and protein binding affinity on intraparticle protein transport in HIC resins. However, this method does not allow the actual protein transport mechanism to be determined because different diffusion models can fit the experimental uptake results equally well even with the diffusivity as the only adjustable parameter. In addition, this method is not recommended for systems in which the uptake is very fast as errors contributed by the particle size distribution and signal detection lag time become significant.

The analytical solutions can accurately predict column breakthrough behavior in HIC systems for most cases by using the isotherms and diffusivities determined from batch uptake experiments. However, they consistently overestimated protein breakthrough in Toyopearl 650S in this study. The reason for this is not understood, but it suggests that protein uptake in suspended resin can be significantly different from that observed in a packed column for some cases. Therefore, it is important to confirm the breakthrough predicted by analytical solutions with experimental results.

The presence of impurities in the feed solution can also affect the accuracy of single-component analytical solutions due to competitive binding or displacement effects. Therefore, it is important to confirm that the load solution is a single-component system when the analytical solutions used in this study are employed. The effect of impurities on column breakthrough behavior seems to be dependent on the resin base matrix, suggesting that the base matrix could play an important role in the breakthrough behavior of multi-component systems.

Acknowledgements

We thank Dr. Steve Dziennik for providing Fortran programs to estimate protein diffusivities from the batch uptake experiments. We are also grateful for support from the National Science Foundation (grant numbers CTS-9977120 and CTS-0350631) and from Merck Research Laboratories for a fellowship to B.C.S.T.

Appendix A. Supplementary data

Supplementary data associated with this article can be found, in the online version, at doi:10.1016/j.chroma.2010.11.051.

References

[1] W.M. Deen, AIChE J. 33 (1987) 1409.
[2] C.N. Satterfield, Mass Transfer in Heterogeneous Catalysis, MIT Press, Cambridge, MA, 1980.
[3] E.M. Renkin, J. Gen. Physiol. 38 (1954) 225.
[4] A. Tongta, A.I. Liapis, D.J. Siehr, J. Chromatogr. A 686 (1994) 21.
[5] J.R. Conder, B.O. Hayek, Biochem. Bioeng. J. 6 (2000) 225.
[6] L.F. Bautista, M. Martinez, J. Aracil, Ind. Eng. Chem. Res. 39 (2000) 4320.
[7] R. Hahn, K. Deinhofer, C. Machold, A. Jungbauer, J. Chromatogr. B 790 (2003) 99.
[8] B.C.S. To, A.M. Lenhoff, J. Chromatogr. A 1205 (2008) 46–59.
[9] M. Simekova, D. Berek, J. Chromatogr. A 1084 (2005) 167–172.
[10] C.A. Brooks, S.M. Cramer, AIChE J. 38 (1992) 1969.
[11] J.C. Bosma, J.A. Wesselingh, AIChE J. 50 (2004) 848.
[12] J. Chen, Y. Sun, J. Chromatogr. A 992 (2003) 29.
[13] F. Xia, D. Nagrath, S.M. Cramer, J. Chromatogr. A 989 (2003) 47.
[14] M.R. Oberholzer, A.M. Lenhoff, Langmuir 15 (1999) 3905.
[15] C. Chang, A.M. Lenhoff, J. Chromatogr. A 827 (1998) 281.
[16] P.M. Armenante, D.J. Kirwan, Chem. Eng. Sci. 44 (1989) 2781.
[17] L.E. Weaver Jr., G. Carta, Biotechnol. Prog. 12 (1996) 342.
[18] A.K. Hunter, G. Carta, J. Chromatogr. A 897 (2000) 81.
[19] J.R. Conder, B.O. Hayek, Biochem. Eng. J. 6 (2000) 215.
[20] G.L. Skidmore, B.J. Horstmann, H.A. Chase, J. Chromatogr. 498 (1991) 113.
[21] A.R. Ozdural, A. Alkan, P.J.A.M. Kerkhof, J. Chromatogr. A 1041 (2004) 77.
[22] S. Yamamoto, Y. Sanom, J. Chromatogr. 597 (1992) 173.
[23] H.A. Chase, J. Chromatogr. 297 (1984) 179.
[24] B.J. Horstmann, H.A. Chase, Chem. Eng. Res. Des. 67 (1989) 243.
[25] D. Whitney, M. McCoy, N. Gordon, N. Afeyan, J. Chromatogr. A 807 (1998) 165.
[26] B.C.S. To, A.M. Lenhoff, J. Chromatogr. A 1141 (2007) 191.
[27] G. Carta, A.R. Ubiera, T.M. Pabst, Chem. Eng Technol. 28 (2005) 1252.
[28] S.R. Dziennik, Ph.D. Thesis, University of Delaware, Newark, DE, USA, 2002.
[29] R.S. Cooper, D.A. Liberman, Ind. Eng. Chem. Fundam. 9 (1970) 620.
[30] K.R. Hall, L.C. Eagleton, A. Acrivos, T. Vermeulen, Ind. Eng. Chem. Fundam. 5 (1966) 620.
[31] R.S. Cooper, Ind. Eng. Chem. Fundam. 4 (1965) 308.
[32] H. Yoshida, T. Kataoka, D.M. Ruthven, Chem. Eng. Sci. 39 (1984) 1489.
[33] N.K. Hiester, T. Vermeulen, Chem. Eng. Sci. 48 (1952) 505.
[34] T. Vermeulen, Ind. Eng. Chem. 45 (1953) 1664.
[35] Q.M. Mao, R. Stockmann, I.G. Prince, M.T.W. Hearn, J. Chromatogr. 646 (1993) 67.
[36] M.A. Fernandez, W.S. Laughinghouse, G. Carta, J. Chromatogr. A 746 (1996) 185.
[37] M.A. Fernandez, G. Carta, J. Chromatogr. A 746 (1996) 169.
[38] J.J. Carberry, AIChE J. 6 (1960) 460.
[39] C.N. Pace, F. Vajdos, L. Fee, G. Grimsley, T. Gray, Protein Sci. 4 (1995) 2411.
[40] A.M. Lenhoff, J. Chromatogr. 384 (1987) 285.
[41] H. Shirahama, J. Lyklema, W. Norde, J. Colloid Interface Sci. 139 (1990) 177.

[42] J.E. Puskas, Y. Dahman, A. Margaritis, M. Cunningham, Biomacromolecules 5 (2004) 1412.
[43] P.E. Stein, A.G.W. Leslie, J.T. Finch, R.W. Carrell, J. Mol. Biol. 221 (1991) 941.
[44] X.M. He, D.C. Carter, Nature 358 (1992) 209.
[45] A. Kondo, S. Oku, K. Higashitani, J. Colloid Interface Sci. 143 (1991) 214.
[46] A. Kondo, F. Murakami, K. Higashitani, Biotechnol. Bioeng. 40 (1992) 889.
[47] J.L. Fogle, J.P. O'Connell, E.J. Fernandez, J. Chromatogr. A 1121 (2006) 209.
[48] G. Carta, A. Ubiera, AICHE J. 49 (2003) 3066.
[49] G.E.P. Box, W.G. Hunter, J.S. Hunter, Statistics for Experimenters. An Introduction to Design, Data Analysis and Model Building, John Wiley & Sons, 1978.
[50] F.G. Smith, W.M. Deen, J. Colloid Interface Sci. 91 (1983) 571.
[51] E.M. Johnson, D.A. Berk, R.K. Jain, W.M. Deen, Biophys. J. 68 (1995) 1561.
[52] H. Yoshida, M. Yoshikawa, T. Kataoka, AIChE J. 40 (1994) 2034.
[53] A.M. Lenhoff, Langmuir 24 (2008) 5991.
[54] D.D. Frey, E. Schweinheim, C. Horvath, Biotechnol. Prog. 9 (1993) 273.
[55] H. Brenner, L.J. Gaydos, J. Colloid Interface Sci. 58 (1977) 312.
[56] S.R. Dziennik, E.B. Belcher, G.A. Barker, A.M. Lenhoff, Biotechnol. Bioeng. 91 (2005) 139.
[57] J. Hubbuch, T. Linden, E. Knieps, J. Thommes, M.R. Kula, Biotechnol. Bioeng. 80 (2002) 359.
[58] A.K. Hunter, G. Carta, J. Chromatogr. A 930 (2001) 79–93.
[59] A.K. Hunter, G. Carta, J. Chromatogr. A 937 (2001) 13–19.
[60] A.C. Awade, T. Efstathiou, J. Chromatogr. B 723 (1999) 69.
[61] R.K. Lewus, G. Carta, AIChE J. 45 (1999) 512.
[62] V.I. Sevastianov, Y.S. Tremsina, R.C. Eberhart, S.W. Kim, in: T.A. Horbett, J.L. Brash (Eds.), Proteins at Interfaces II. Fundamentals and Applications, ACS Symposium Series 602, 1995 (Chapter 14).